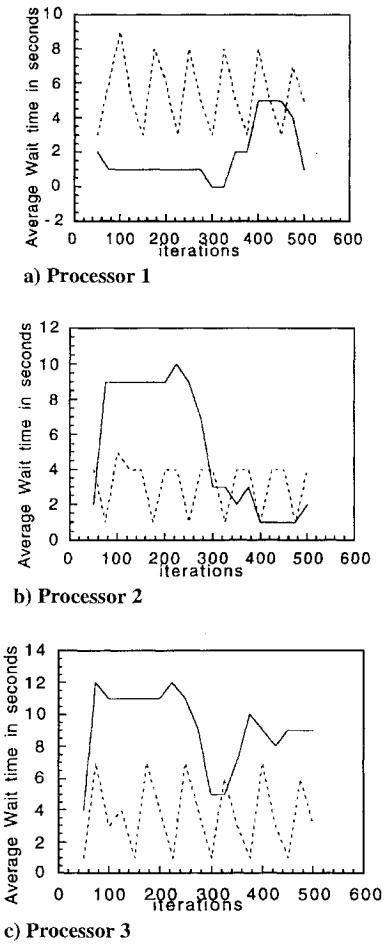

Fig. 4 Comparison of wait times of PVM nodes in a heavily loaded network: - - - -, dynamic balance and ——, static balance.

Concluding Remarks

An existing Navier–Stokes solver has been modified using the PVM software to compute flowfields in parallel using the network-based parallel computer. Excellent speedup in computation time was obtained using the parallel computations on a network of three workstations. The computation speed using the present network parallel computer was about 20% of that of a single processor of a Cray Y–MP supercomputer for the present application and the grid size. A simple dynamic load balancing algorithm was implemented to improve the performance of parallel computation.

Acknowledgments

This work was supported by the U.S. Army Research Office under the Center of Excellence in Rotorcraft Technology program. Thomas Doligalski was the Technical Monitor.

References

[1]Smith, M. H., "Distributed Parallel Flow Solutions Using Overset Grids," *Proceedings of the NASA Workshop on Distributed Computing for Aerosciences Applications*, 1993.

[2]Beguelin, A., Dongarra, J., Geist, A., Manchek, R., and Sunderam, V., "A User's Guide to PVM—Parallel Virtual Machine," Oak Ridge National Lab., ORNL/TM-11826, Oak Ridge, TN, March 1992.

[3]Smith, M., and Pallis, J., "MEDUSA—An Overset Grid Flow Solver for Network-Based Parallel Computer Systems," AIAA Paper 93-3312, July 1993.

[4]Weed, R. A., and Sankar, L. N., "Computational Strategies for Three-Dimensional Flow Simulations on Distributed Computer Systems," AIAA Paper 94-2261, June 1994.

[5]Wake, B. E., and Sankar, L. N., "Solution of Navier–Stokes Equations for the Flow Over a Rotor Blade," *Journal of the American Helicopter Society*, Vol. 34, April 1989, pp. 13–23.

[6]Bangalore, A., Tseng, W., and Sankar, L. N., "A Multi-zone Navier–Stokes Analysis of Dynamic Lift Enhancement Concepts," AIAA Paper 94-0164, Jan. 1994.

Bow Shock/Jet Interaction in Compressible Transverse Injection Flowfields

M. R. Gruber* and A. S. Nejad†
U.S. Air Force Wright Laboratory, Wright–Patterson Air Force Base, Ohio 45433
T. H. Chen‡
Taitech, Inc., Beavercreek, Ohio 45440
and
J. C. Dutton§
University of Illinois at Urbana–Champaign, Urbana, Illinois 61801

Introduction

TRANSVERSE injection of a gaseous fuel stream into a supersonic flow appears schematically in Fig. 1. This sketch illustrates the features of the flowfield in a plane through the spanwise jet centerline, where a three-dimensional bow shock forms ahead of the jet and interacts with the approaching turbulent boundary layer, resulting in separation. Previous investigations of this flowfield have provided clear visualizations of the large-scale vortices formed at the interface between the freestream and injectant fluids.[1–3] These eddies influenced the position of the bow shock.[2] Some images also showed the region enclosed by the separation shock where the bow shock and turbulent boundary layer interact.[1,2] This region contains locally high wall static pressures as found in both experiments[4] and numerical predictions.[5] Numerical investigations of a reacting transverse hydrogen jet in a supersonic airstream by Takahashi and Hayashi[6] showed relatively high static temperatures occurring within this separated zone. Erosion of the injector wall could occur as a result of this local high temperature zone.

The objective of the present work is to investigate the interaction between the upstream shock structure and the interfacial eddies in the jet fluid. The influence of injector geometry on the separation shock is also of interest. Both issues are addressed using a planar laser-based visualization technique to capture instantaneous images of the interaction created by circular and elliptical injectors fueled with air. Details regarding the facility and imaging technique used are available elsewhere.[7,8] Table 1 shows geometric features of the two injectors studied.

Results and Discussion

The freestream conditions were set such that $M_\infty = 1.98$, $p_{0,\infty} =$ 317 kPa, and $T_{0,\infty} = 300$–302 K. Jet flow conditions were set so that the jet-to-freestream momentum flux ratio J,

$$J = \frac{(\rho u^2)_j}{(\rho u^2)_\infty} = \frac{(\gamma p M^2)_j}{(\gamma p M^2)_\infty} \tag{1}$$

was identical in each case ($J = 2.90$). This parameter controls jet penetration into the crossflow.[1,9] Images were obtained for both circular and elliptical injection using air, cases C1A and E1A, with the major axis of the ellipse aligned with the freestream flow.

Instantaneous images from cases C1A and E1A appear in Figs. 2 and 3, respectively. Freestream fluid (light) flows from left to right, and the jet fluid (dark) enters from the lower edge (jets are centered at $x/d_{\text{eff}} = 0$). All of the images presented show some boundary-layer

Received Jan. 26, 1996; revision received Feb. 28, 1996; accepted for publication March 15, 1996. This paper is declared a work of the U.S. Government and is not subject to copyright protection in the United States.

*Aerospace Engineer, Advanced Propulsion Division, WL/POPT. Member AIAA.
†Senior Research Engineer, Advanced Propulsion Division, WL/POPT.
‡Senior Research Scientist. Senior Member AIAA.
§Professor, Department of Mechanical and Industrial Engineering. Associate Fellow AIAA.

Table 1 Injector geometries

Injector	Semimajor axis a, mm	Semiminor axis b, mm	Effective diameter d_{eff}, mm	Eccentricity ε
Circular (case C1A)	3.18	3.18	6.35	0
Elliptical (case E1A)	6.25	1.63	6.35	0.97

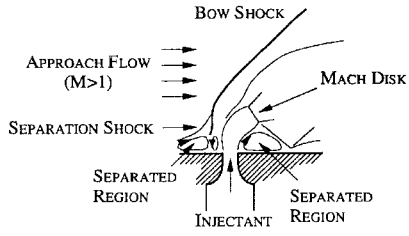

Fig. 1 Transverse injection flowfield schematic.

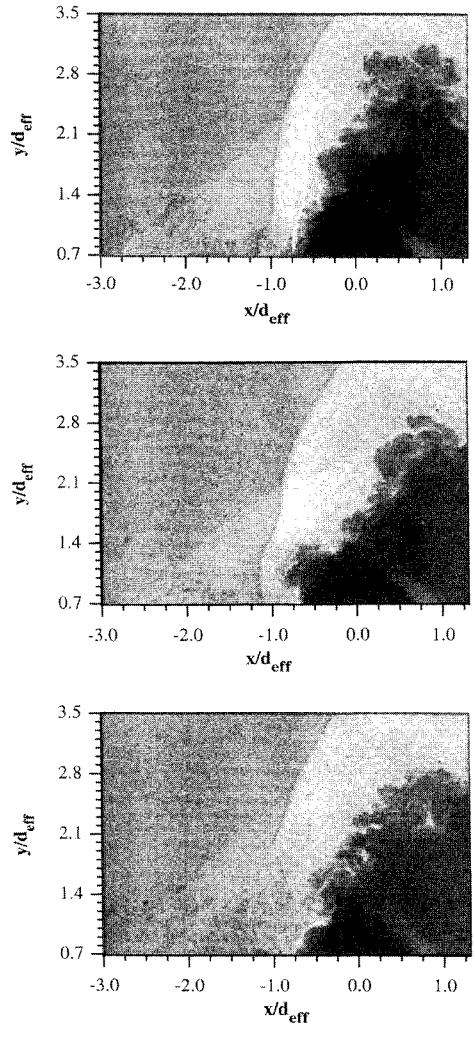

Fig. 2 Instantaneous images of circular injection using air (case C1A).

fluid along the lower edge as it enters the region beneath the separation shock wave. Several other features can be easily observed, including the bow shock standoff distance (i.e., the distance upstream of the injector leading edge where the bow shock intersects the lower edge of the image) and the streamwise (x) and transverse (y) dimensions of the upstream separation shock wave.

In Fig. 2 (case C1A), the bow shock's behavior below the point of intersection with the separation shock appears strongly influenced by the structures formed after the jet fluid enters the crossflow. In-

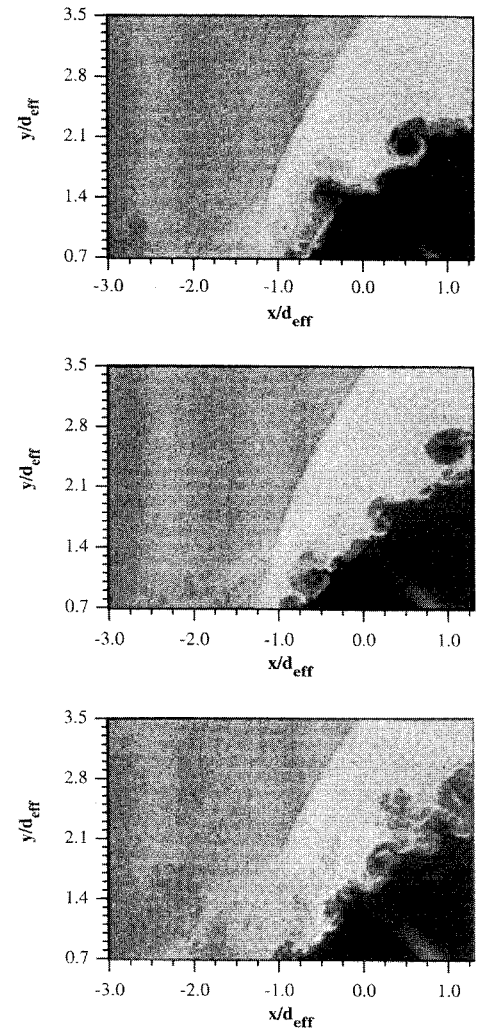

Fig. 3 Instantaneous images of elliptical injection using air (case E1A).

stantaneous visualizations in which large eddies do not appear near the wall show the bow shock being essentially normal to the wall. In contrast, the second image of Fig. 2 contains an eddy at roughly $y/d_{\text{eff}} = 1$. In response to this feature, the bow shock curves sharply upstream, increasing its distance from the injector centerline. Another interesting occurrence is shown in the third image, where the shock apparently lifts higher off the wall, allowing the boundary layer and jet fluids to mix subsonically upstream of the jet exit. This periodic lifting, caused when the approaching boundary layer is relatively thick and the sonic line occurs at a higher elevation off the wall, probably exacerbates the hot-spot phenomenon associated with reacting injection flowfields since fuel propagates farther upstream. Despite the dynamic nature of the bow shock's behavior below the intersection with the separation shock, a standoff distance of about 0.5 d_{eff} consistently occurs. Above the intersection point, fluctuations in the bow shock's position also occur, although no dramatic curvature changes appear. In all of the images obtained from case C1A, the bow shock intersected the top edge of the image, $y/d_{\text{eff}} = 3.5$, between $-0.50 \leq x/d_{\text{eff}} \leq 0$.

The region between the bow and separation shocks is an important feature in transverse injection flowfields in relation to its flame-holding capability in combusting situations. At the spanwise centerline of the jet/crossflow interaction, two points describe the extent of the separation shock. The first point is upstream of the injector where the separation shock intersects the bottom edge of the image. The second point is the intersection of the bow and separation shocks that defines the highest transverse elevation of this region. In the ensemble of images collected for case C1A, the position of the first point falls between $-3.0 \leq x/d_{\text{eff}} \leq -2.25$, whereas the location of the second point varies from about 1.6 to 2.8 effective diameters above the bottom wall.

Figure 3 shows the instantaneous images obtained from case E1A. Large-scale eddies formed at the edge of the jet near the injector wall influence the behavior of the bow shock below the point of intersection with the separation shock in case E1A, though not to the degree that was observed in Fig. 2. The images in Fig. 3 give some evidence of the curvature changes induced by the eddies. Also, the third image shows the shock lifting phenomenon that appeared in case C1A. The bow shock standoff distance is approximately $0.25d_{\text{eff}}$ (50% closer to the injector leading edge than for case C1A). This smaller standoff distance is explained by the asymmetric vortex development associated with the elliptical injector geometry leading to more rapid spreading in the minor-axis direction than in the major-axis direction.[10] Apparently, the jet fluid expands more in the spanwise direction (z) than in the streamwise direction (x) at the exit plane of the elliptical nozzle, allowing the shock to stand closer to the jet exit and still accomplish the necessary pressure correction. In the region above the point of intersection of the bow and separation shocks, small fluctuations in the bow shock's position occur. However, the images shown in Fig. 3 indicate a weaker bow shock in case E1A than in case C1A as inferred by its slope. The ensemble of images obtained for case E1A indicates that the bow shock intersects the upper edge of the image at streamwise positions between $-0.25 \leq x/d_{\text{eff}} \leq 0$. Thus, in addition to being weaker than the wave in case C1A, the bow shock in case E1A fluctuates over a smaller spatial range.

The upstream extent of the separation shock in case E1A falls between $-2.75 \leq x/d_{\text{eff}} \leq -1.75$, whereas the point of intersection of the bow and separation shocks is between 1.1 and 2.1 effective diameters above the bottom wall. These values are significantly lower than those obtained from case C1A; thus, the area beneath the separation shock associated with the elliptical injector is smaller than in circular injection at the spanwise centerline of the jet/crossflow interaction. Therefore, injection through the elliptical nozzle potentially reduces any hot-spot phenomenon associated with injection through a circular nozzle oriented perpendicular to the supersonic freestream.

Conclusions

In flowfields created by transverse injection into supersonic crossflows, the bow and separation shocks formed upstream of the injectant plume are dominant features. In the present investigation, the interaction between these features and the large-scale eddies that develop at the jet/freestream interface has been examined. Results indicate that the large structures strongly influence the near-wall behavior of the bow shock, often resulting in severe curvature changes and positional fluctuations. The eddies exert a weaker influence on the bow shock further away from the wall. Lifting of the bow shock has been observed when the approaching boundary layer is relatively thick. In these instances, injectant and freestream fluid mix subsonically upstream of the injector orifice, thereby exacerbating the hot-spot phenomenon found in reacting transverse injection flowfields. Finally, the injector geometry strongly affected the upstream separation zone, the bow shock standoff distance, and the strength of the bow shock. Elliptical injection with the major axis aligned with the freestream flow resulted in a smaller separation zone and standoff distance and a weaker bow shock compared with circular injection.

References

[1]Gruber, M. R., Nejad, A. S., Chen, T. H., and Dutton, J. C., "Mixing and Penetration Studies of Sonic Jets in a Mach 2 Freestream," *Journal of Propulsion and Power*, Vol. 11, No. 2, 1995, pp. 315–323.

[2]Gruber, M. R., Nejad, A. S., and Dutton, J. C., "Circular and Elliptical Transverse Injection into a Supersonic Crossflow—The Role of Large-Scale Structures," AIAA Paper 95-2150, June 1995.

[3]Van Lerberghe, W. M., "Large-Scale Structure and Mixing in a Sonic Transverse Jet Injected into a Supersonic Crossflow," Ph.D. Thesis, Dept. of Mechanical and Industrial Engineering, Univ. of Illinois at Urbana–Champaign, Urbana, IL, 1995.

[4]Everett, D. E., Dutton, J. C., and Morris, M. J., "Pressure-Sensitive Paint Measurements of the Pressure Field About a Sonic Jet Injected Transversely into a Mach 1.6 Freestream," AIAA Paper 95-0524, Jan. 1995.

[5]Dhinagaran, R., and Bose, T. K., "Two-Dimensional Jet Interaction Flowfield Predictions with an Algebraic Turbulence Model," AIAA Paper 95-2242, June 1995.

[6]Takahashi, M., and Hayashi, A. K., "Numerical Study on Mixing and Combustion of Injecting Hydrogen Jet in a Supersonic Air Flow," AIAA Paper 91-0574, Jan. 1991.

[7]Gruber, M. R., and Nejad, A. S., "New Supersonic Combustion Research Facility," *Journal of Propulsion and Power*, Vol. 11, No. 5, 1995, pp. 1080–1083.

[8]Gruber, M. R., "An Experimental Investigation of Transverse Injection from Circular and Elliptical Nozzles into a Supersonic Crossflow," Ph.D. Thesis, Dept. of Mechanical and Industrial Engineering, Univ. of Illinois at Urbana–Champaign, Urbana, IL, 1996.

[9]Papamoschou, D., and Hubbard, D. G., "Visual Observations of Supersonic Transverse Jets," *Experiments in Fluids*, Vol. 14, 1993, pp. 468–476.

[10]Ho, C., and Gutmark, E., "Vortex Induction and Mass Entrainment in a Small-Aspect-Ratio Elliptic Jet," *Journal of Fluid Mechanics*, Vol. 179, 1987, pp. 383–405.

Proving Algorithm Symmetry for Flows Exhibiting Symmetry Breaking

Raja Sengupta* and Paul D. Orkwis†
University of Cincinnati, Cincinnati, Ohio 45221–0070

Introduction

THIS Note is prompted by the need to demonstrate the symmetry of the conical Navier–Stokes algorithm used by Dusing and Orkwis[1] in studying the formation of vortex asymmetry in flows over cones at incidence. Algorithm-related asymmetry because of approximate factorization has been demonstrated previously for the Beam–Warming algorithm in its diagonal form by Levy et al.[2] The symmetry of the current algorithm was studied to avoid similar spurious computations.

In general, this issue is important whenever flows that involve symmetry breaking are under consideration, namely, flow over a cone, flow over a circular cylinder, flow in a divergent nozzle of rectangular cross section, flow along a corner, and so forth.[3–6] These flows undergo bifurcation at some critical value of a parameter (or combination of parameters), e.g., Reynolds number in the cylinder case, divergence angle in the nozzle case. Numerical simulations can provide disturbance-free base flows for studying the stability properties of the symmetric flow only if the algorithm employed in the simulation is free from asymmetric bias. In other words, we expect to capture the symmetric solution using a bias-free algorithm, given symmetric initial and boundary conditions. However, this would be possible only in the absence of round-off errors. For the purposes of reliable linear stability analyses of symmetric base flows, solutions converged close to machine accuracy are still acceptable, but it is necessary to employ a symmetric algorithm to achieve this. It is therefore imperative that algorithm symmetry be ensured before such calculations are attempted. This can be done analytically, and a simple illustration is presented.

In this Note, the case of flow over a cone at an angle of attack is considered. The thin-layer Navier–Stokes (TLNS) equations are to be solved on a conical grid using the two-step approximate factorization scheme of Anderson[7] as modified by Vanden and Belk.[8] Further details of the algorithm can be found in Ref. 1. The goal of this Note is to check the symmetry of the algorithm by analytical means. To this effect, the symbolic manipulation software MACSYMA is used in part.

Received Sept. 19, 1995; revision received Jan. 17, 1996; accepted for publication Jan. 18, 1996.

*Graduate Research Assistant, Department of Aerospace Engineering and Engineering Mechanics. Student Member AIAA.

†Assistant Professor, Department of Aerospace Engineering and Engineering Mechanics. Senior Member AIAA.